Journal of Sound and Vibration (1999) **227**(5), 965–978
Article No. jsvi.1999.2055, available online at http://www.idealibrary.com on IDEAL®

ENLARGEMENT OF OUT-OF-ROUND WHEEL PROFILES ON HIGH SPEED TRAINS

Dr. B. MORYS

Fraunhofer Institut Informations- und Datenverarbeitung IITB, *Fraunhoferstr*. 1, *D*-76131 *Karlsruhe*, *Germany*

(*Accepted* 22 *September* 1998)

Radial deviations from the ideal round shape of railway wheels and out-of-round (OOR) phenomena more generally have been a well known problem for a long time. Since the typical speed range of modern high speed trains have become higher and the newer building substructures "stiffer", in some vehicles both a disturbing, humming noise within the passenger compartment at high speeds and an increase of maintenance costs due to OOR wheel shapes can be observed. Measurements show that small radius deviations of some typical OOR shapes enlarge rapidly. In order to analyze the origin and the enlargement of OOR phenomena a vehicle–track model was developed to describe the short term system dynamics of an ICE-1 carriage. While running on an elastic track, disturbances by wheel radius deformations are assumed. In a second step, this model was extended by an iterative long term wear model to analyze the changes in radius deviations over a long operating period. Simulation results show that OOR wheel shapes cause extensive variations in normal forces on stiff substructures at high speeds. Under realistic operating conditions even a periodical wheel–rail lift-off can be observed. The normal force variations accelerate the wheel vertically and excite a bending oscillation of the wheelset axle which leads to lateral slip and lateral material excavation. Subsequently, the location and amplitude of the two excavation maxima—for the positive and negative maximum of the lateral slip—within the tread were investigated. Their locations change as a function of vertical track properties as well as of the excitation frequency which is the product of the rotation frequency of the wheel and the number of OOR periods over the wheel circumference (OOR order). It is shown that under specific operating conditions only some OOR shapes enlarge while others lead to higher harmonic orders.

1. INTRODUCTION

OOR phenomena on wheels of track-guided vehicles have been well known for a long time. Even after a short time of running, the first deviations from the ideal round wheel shape can be detected. These deviations enlarge rapidly during further operation. Figure 1 shows a typical radius deviation with the third order OOR shape measured on a steel wheel of the BA-14 type from an ICE-1 carriage. Generally, typical shapes of deformation depend on operating

0022–460X/99/450965 + 14 $30.00/0

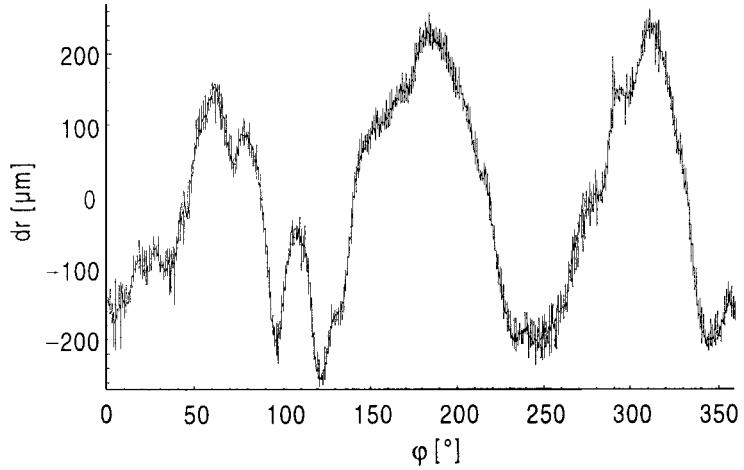

Figure 1. Typical deviation of a wheel radius (third order OOR shape).

conditions such as speed range, track properties, etc. At high speeds (>200 km/h) OOR wheels cause considerable vibrations within a frequency range of 70–100 Hz. These vibrations are transmitted from the wheels via the bogies to the passenger compartments, where they are perceived as a disturbing, humming noise. In addition to the deterioration of comfort, maintenance costs are increased by this phenomenon.

The goal of this paper is to explain the enlargement mechanism leading to the growth of small deviations due to manufacturing/maintenance tolerances and/or other origins as discussed in reference [1]. Material inhomogeneity within the wheel tread is not taken into account. It is shown that in the presence of specific operating conditions only some OOR orders enlarge rapidly whereas others change their shape and lead to higher OOR orders.

2. MODEL

In order to analyze the reinforcement of OOR phenomena at high speeds a modelling strategy comprising two steps was chosen: within the first step a

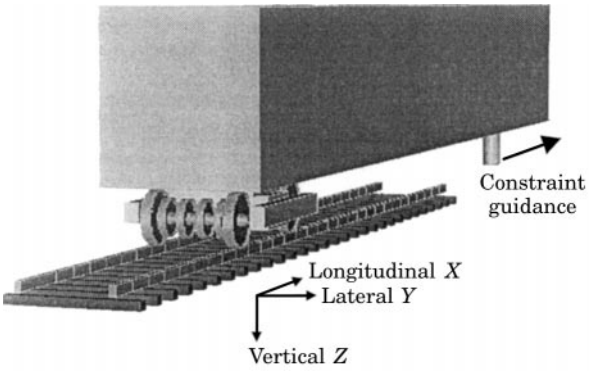

Figure 2. Overview of vehicle–track model.

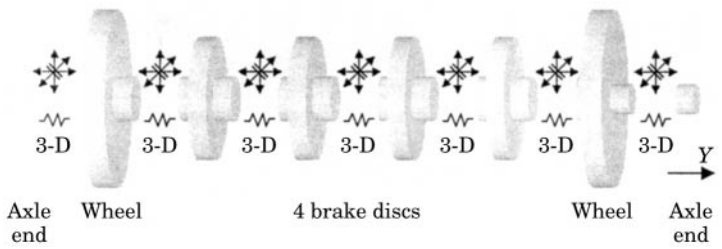

Figure 3. Model of the BA-14 wheelset type consisting of 8 rigid bodies (2 wheels, 4 brake discs and 2 axle ends) without translational degrees of freedom, coupled by 3-dimensional rotational spring damper elements.

realistic 3D model of an ICE-1 carriage running on an elastic track was developed to simulate the short term system dynamics. In a second step the model was extended to an iterative long term wear model to analyze the changes of radial deviations (OOR shapes) within a long operating period.

2.1. VEHICLE–TRACK MODEL

The short term system dynamics model represents one half of an ICE-1 carriage including one typical bogie of the MD-530 type and two standard wheelsets of BA-14 type running on an elastic, effectively infinite track (see Figure 2). For the wheelsets, the wheel-rail contact and the substructure complex physical descriptions were used, while the car body and the bogie were modelled rather simply. The whole model is implemented within the ADAMS simulation environment [2].

2.1.1. *Wheelset BA-14 with bending and torsional elasticity*

Each wheelset consists of 8 rigid bodies (2 wheels, 4 brake discs and 2 axle ends) as shown in Figure 3. All translational degrees of freedom between two adjacent wheelset elements are constrained as indicated by the double crossed out arrows. Three dimensional rotational spring damper elements between the rigid bodies introduce the bending and torsional elasticity.

The parameters were validated by comparing calculated and measured natural frequencies of a ''free'' wheelset (see Table 1 [3]). Measurements were made by hanging the wheelset from a chain attached to the end of the axle. There is excellent agreement between calculated and measured values of the first bending and torsional natural frequencies. These are within the range of the humming noise caused by the OOR phenomenon, and are therefore in the frequency range of interest.

2.1.2. *Wheel–rail contact*

The tread of each wheel has the transverse profile S1002. OOR shapes are modelled by a variable radius around the tread as a function of the angle of wheel rotation φ. The variable circumferential radius at the centre of the transverse profile $r_0(\varphi)$ is defined for each wheel independently by a two

TABLE 1

Measured and calculated natural frequencies of the wheelset type BA-14

Eigenmode	Measured (Hz)	Calculated (HZ)	Δf_{EF} (%)
1. bending	82	82·0	0
1. torsion	96	95·9	0
2. bending	162	182·0	+12
3. bending	215	353·7	+65
2. torsion	289	319·2	+10

dimensional list of discrete points (φ_i, r_{0i}) which are interpolated linearly. This offers the flexibility to use measured or generated radius shapes.

For the wheel–rail contact a coupling element [4] including the elastic properties of the profiles, multiple contact patches and the simplified theory of contact by Kalker implemented in FASTSIM [5, 6] is used. It was extended for the calculation of the wear energy within the wheel–rail contact patches.

2.1.3. *Substructure*

On the assumption that the vehicle–track interaction takes place mainly within a track section in a certain environment of the vehicle only this section is modelled as dynamically active while the remaining track section is assumed to be dynamically inactive (see Figure 4). The left and right rails within the dynamically active track section are described by two massless Euler–Bernoulli beams for the lateral and vertical direction respectively. Their supported start and end points $X_{BeamStart}$ and $X_{BeamEnd}$ are moving with the vehicle in such a way that the bogie is centred between them. The discrete bedding of the rails is realized by track modules (TM). When the distance between the beam end point and the last track module becomes small, the TM is effectively excluded from

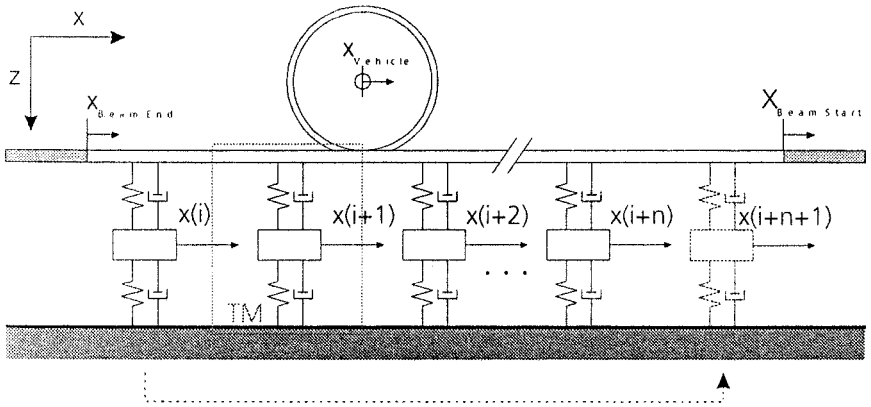

Figure 4. Implementation of the dynamical active part of an infinite, discrete bedded substructure synchronized with the vehicle position.

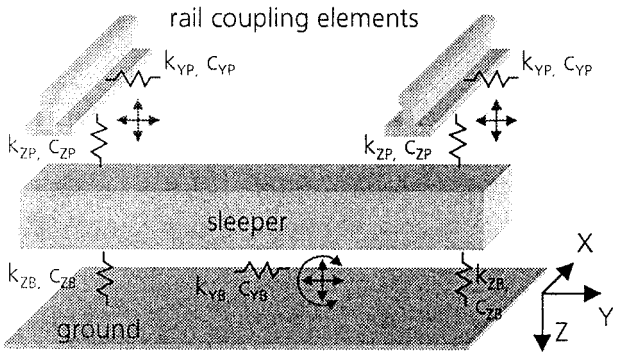

Figure 5. Structure of a track module (TM).

calculation of the beam equation, moved in front of the first TM and included again into the calculation.

Each track module (see Figure 5) consists of three rigid bodies: two rail coupling elements which are connected to the beams and contain the proportionate rail mass and one sleeper. The rail coupling elements each have a lateral and vertical translational degree of freedom related to the sleeper. The pad is described by two translational spring damper elements. The sleeper has related to the ground a lateral and vertical translational degree of freedom as well as a rotational to the X-axis. The ballast is modelled by one lateral and two vertical translational spring damper elements.

"Stiff" and "soft" substructures are considered by two corresponding parameter sets which resemble the modern high speed tracks ("stiff") and the former substructures ("soft") of the Deutsche Bahn AG [7–9].

2.2. ITERATIVE LONG TERM WEAR MODEL

To predict the long term changes of profile from the results of several short term system dynamic analyses, an iterative long term wear model was developed. It is based on the hypothesis that the mass excavation Δm at each point of the wheel circumference is proportional to the wear energy W_R within the contact patch at that point, different proportionality factors $k(P_{RA})$ for "mild" and "heavy" wear being assumed [10], depending on the wear power per unit area of the contact patch P_{RA}:

$$\Delta m = k(P_{RA})W_R,$$

$$k(P_{RA}) = \left\{ \begin{array}{ll} 3\times10^{-9}\text{kg/J},\ P_{RA}\leq 4\times10^{6};\text{W/m}^2, & \text{mild wear} \\ 2\times10^{-8}\ \text{kg/J},\ P_{RA} > 4\times10^{6}\ \text{W/m}^2, & \text{heavy wear} \end{array} \right\} \quad (1)$$

$$\Delta r_{Wear} = c \quad \frac{\Delta m}{\rho a}. \quad (2)$$

The radius reduction Δr_{Wear} is calculated according to equation (2), where ρ is the material density, and a is the area of the mainly used part of the tread. The

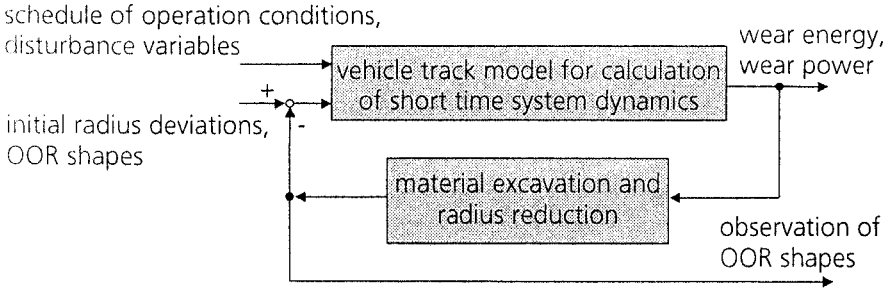

Figure 6. Principle of the iterative long term wear model.

roll-over factor c denotes the number of wheel rotations which are taken into account.

The iterative long term wear model calculates the changes of the OOR shapes over periods of thousands of kilometres in the following way as illustrated in Figure 6: At the beginning of a long term wear simulation an initial OOR shape for each wheel, disturbance variables (i.e. imbalanced wheelset masses) and a schedule of operating conditions (speed, vehicle direction, track properties) are selected. With these initial parameters a short term system dynamic analysis is performed. From the results after the end of the transient behaviour (i.e. wear energy, wear power within the wheel–rail contact patch, etc.) the material excavation and the radius reduction for each point on the wheel circumference are obtained by the material excavation hypothesis. Then, the OOR shapes are modified by the previously calculated radius reduction and taken as new initial parameters. Thus, the long term changes of the OOR shapes are calculated iteratively.

To get more realistic results, some model parameters (speed, vehicle direction and track properties) are changed from one iteration to another according to a

TABLE 2

Representative schedule of operating conditions for high speed trains

#	Vehicle speed (m/s)/(km/h)	Direction Vehicle	Substructures characteristics
1	70/252	forward	stiff
2	60/216	backward	stiff
3	50/180	forward	stiff
4	70/252	backward	stiff
5	60/216	forward	stiff
6	50/180	backward	stiff

representative schedule of operating conditions. Table 2 shows the schedule of operating conditions which was used to calculate the results described below.

3. ANALYSIS

3.1. NORMAL FORCES WITHIN THE CONTACT PATCH

In order to understand the long term wear behaviour the short term system dynamics has to be investigated. At the outset the normal force variations between wheel and rail dF_N caused by five different sinusoidal radius deformations with one, two, three, four and five periods per circumference (first, second, third, fourth and fifth OOR order) and a peak-to-peak OOR amplitude $r_{OOR} = 0{\cdot}2$ mm (manufacturing tolerance) are investigated. The system dynamics are compared for the two described different track properties "stiff" and "soft" and three different speeds $V_x = 50$, 60 and 70 m/s, but with track irregularities being neglected.

The term "*amplitude*" is defined here to be half the difference between the maximum and minimum value of a nearly sinusoidal curve. The term "*phase*" of a curve is defined as the lead of the maximum of this curve on the maximum of the radius deviation multiplied by 360 degrees and related to the period of the excitation frequency f_{OOR} (see Figure 9, of section 3.2). The excitation frequency f_{OOR} is defined as the product of the frequency of wheel rotation f_Y and the OOR order n_{OOR}.

Although the dynamics of the whole vehicle–track system are strongly non-linear, the variation in normal force and the lateral slip are—under the assumption of small radius deviations—nearly a linear function of the OOR amplitude. The influence of the discrete bedding on the variation in normal force and the lateral slip is negligible. After the end of the transient period the system dynamics show nearly a stationary behaviour: e.g. the system dynamics and the wear within the tread can be expressed by a time-independent function of the angle of wheel rotation φ.

In Figure 7 the amplitude (left graph) and phase (right graph) of the normal force variation dF_N on a "stiff" substructure are shown as a function of

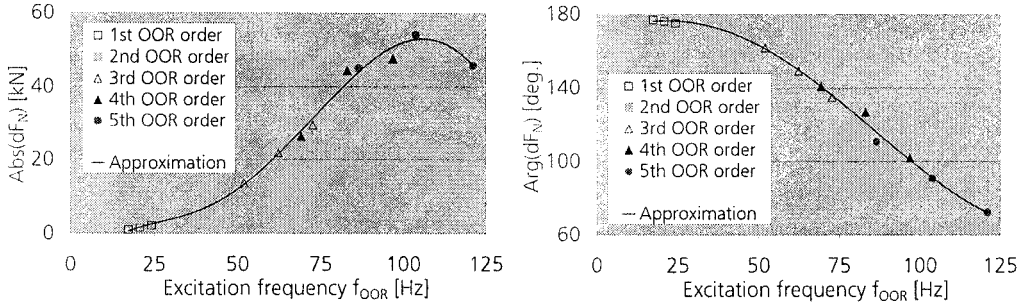

Figure 7. Amplitude and phase of the normal force variation caused by wheels with OOR orders from 1 to 5 and an radius deviation $r_{\mathrm{OOR}} = 0{\cdot}2$ mm on *stiff track* in dependency on the excitation frequency f_{OOR}. OOR orders: □: 1; ▩: 2; △: 3; ▲: 4; ●: 5; —: Approximation.

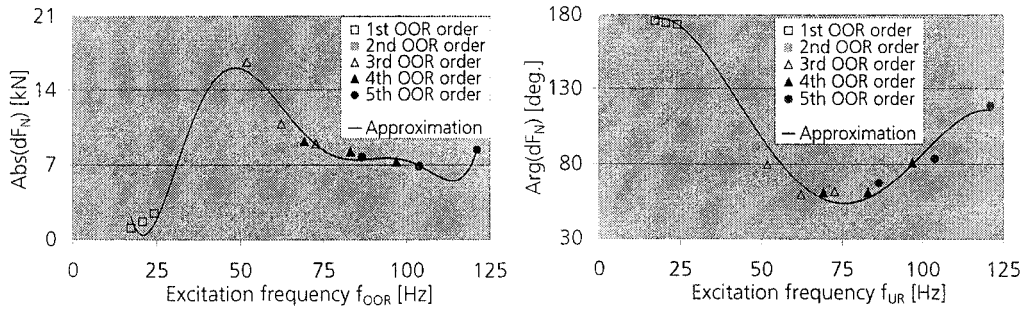

Figure 8. Amplitude and phase of the normal force variation caused by wheels with OOR orders from 1 to 5 and an radius deviation $r_{OOR} = 0{\cdot}2$ mm on *soft track* in dependency on the excitation frequency f_{OOR}. Key as Figure 7.

the excitation frequency f_{OOR}. The results are calculated in the time domain as necessary for non-linear systems. The calculated values of the functions are approximated by best-fit polynomials. The behaviour of the system depends mainly on the excitation frequency instead of on the rotational frequency of the wheel. For the typical frequency range of the humming noise between 75 and 100 Hz which is excited by the third and the fourth order OOR shapes at the typical speed of 250 km/h, very large normal force variations can be observed. Under these realistic operating conditions a periodical wheel–rail lift-off can be observed for peak-to-peak deviations in radius of greater than 0·5 mm. This is within the operating tolerance of $r_{OOR} = 0{\cdot}6$ mm. According to the phase–frequency characteristic the maximum normal force occurs for low frequencies at the radius minimum. For higher frequencies it is shifted to the rising slope of the radius curve.

In the case of soft track properties (see Figure 8) the maximum normal forces are significantly smaller and show a resonance frequency at about 50 Hz. With increasing excitation frequency the amplitude of the normal force variation decreases slightly. A wheel–rail lift-off within the operating tolerances cannot be recognised.

3.2. THE MECHANISM OF OOR ENLARGEMENT

Due to large variations in the normal forces the wheel is accelerated vertically. The vertical wheel displacement excites a bending oscillation of the wheelset axle. The wheel disk can be assumed to be stiff and rigidly coupled to the axle within the frequency range below 200 Hz. Hence a bending oscillation of the axle causes wheel disk vibrations which induce lateral slip and, consequently, lateral material excavation. Simulations show that this effect is dominant in the OOR enlargement. Longitudinal material excavation as a consequence of longitudinal slip and spin plays a minor role.

In Figure 9, typical simulation results are presented for the case of a vehicle running along a stiff track at a speed of 70 m/s with an OOR shape of the third order and $r_{OOR} = 0{\cdot}3$ mm at all wheels. The curve of the wear energy W_R shows two maxima per period of the radius deviation dr. The first maximum W_{RMax1} is

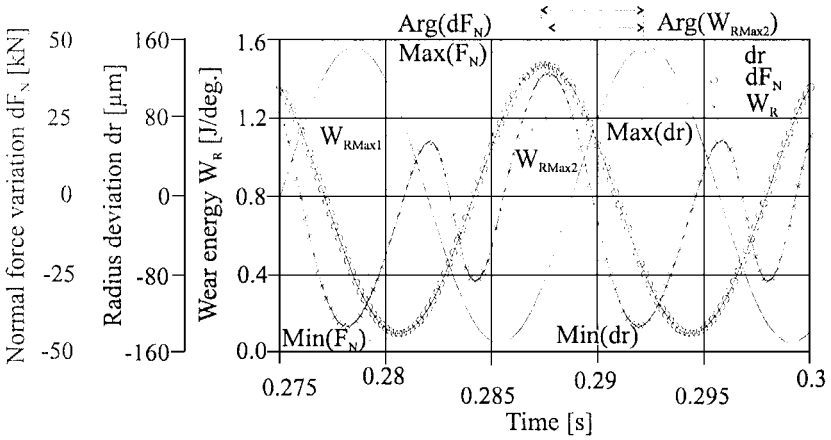

Figure 9. Wear energy W_R, normal force variation dF_N and wheel radius deviation dr (V_X = 70 m/s OOR third order, r_{OOR} = 0·3 mm, stiff track).

caused by the positive maximum of the lateral slip, v_Y, and the second maximum W_{RMax2} by the negative maximum of v_Y. In sections 3.2.1 and 3.2.2 the position of the two wear energy maxima and excavation maxima on the wheel circumference relative to the OOR shape is discussed as a function of excitation frequency, peak-to-peak OOR amplitude r_{OOR} and normal force variation.

3.2.1. *Effect of excitation frequency*

In the case of low excitation frequencies ($f_{OOR} < 40$ Hz) the phase of W_{RMax1} is about $+30°$, and of W_{RMax2} about $+210°$ relative to the maximum of the dr curve (see Figure 10). The first excavation maximum is located on the rising radius slope before its maximum, and the second on the failing radius curve before its minimum. With increasing f_{OOR} a growing phase lag occurs: W_{RMax1} is shifted to the maximum of the dr curve and further on to the failing slope while

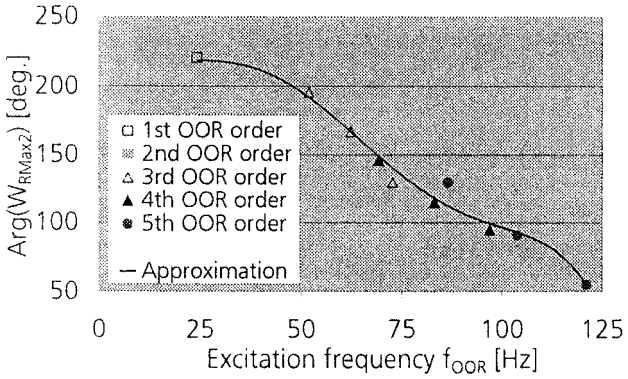

Figure 10. Phase of the second maximum of the wear energy W_{RMax2} caused by wheels with OOR orders from 1 to 5 and an radius devation r_{OOR} = 0·2 mm on *stiff track* in dependency on the excitation frequency f_{OOR}. Key as Figure 7.

W_{RMax2} is moved firstly to the minimum of the radius curve and afterwards to the rising slope (see Figure 10).

3.2.2. *Effects of OOR amplitude and normal load*

For small radius deviations the amplitudes of the normal force variations, of the wheelset axle bending oscillation and of the lateral slip, show a proportionality to the OOR amplitude. Their phase relation relative to the radius curve is not affected by a change of the OOR amplitude: the system behaves linearly.

Up to this point the change in amplitude of the two maxima of the wear energy which is assumed to be proportional to the material excavation has not been discussed. The amplitude of the dominant lateral wear energy within the contact patch is mainly determined by the lateral slip v_Y, the lateral tangential force induced by v_Y and the normal force. It is apparent in Figure 9 that the minimum of the normal force $Min(F_N)$ coincides approximately with the first maximum of the wear energy W_{RMax1} as well as the maximum of the normal force $\mathrm{Max}(F_N)$ with W_{RMax2}. Consequently, W_{RMax1} is much smaller than W_{RMax2} although the absolute value of the positive and negative maxima of the lateral slip are similar. For an increase of normal force variations W_{RMax2} is growing rapidly caused by the coincidence of increasing amplitude of the lateral slip as well as of the maximum of the normal force while the changes in W_{RMax1} are small because of the antagonistic increase of the amplitude of lateral slip and the decrease of normal force.

3.3. LONG TERM WEAR DEVELOPEMENT

In Figures 11–14 four typical results of long term wear analyses are shown. They are based on sinusoidal initial wheel radius deviations of the first, the second, the third and the fourth OOR order with a peak-to-peak OOR amplitude of $r_{OOR} = 0.2$ mm. In each of these figures the left graph shows the different radius deviations *dr* during the wear progress from the initial profile at the top to the last profile at the bottom as a function of the angle of wheel

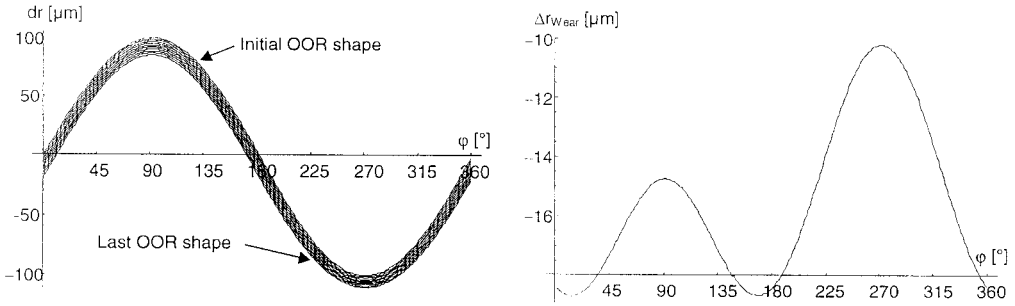

Figure 11. Long term wear development shown by the wheel shape changes dr (left graph) and the radius reduction Δr_{Wear} (right graph) as a function of the angle of wheel rotation φ as a consequence of an initial OOR wheel shape of the first order and peak-to-peak radius deviation $r_{OOR} = 0{\cdot}2$ mm.

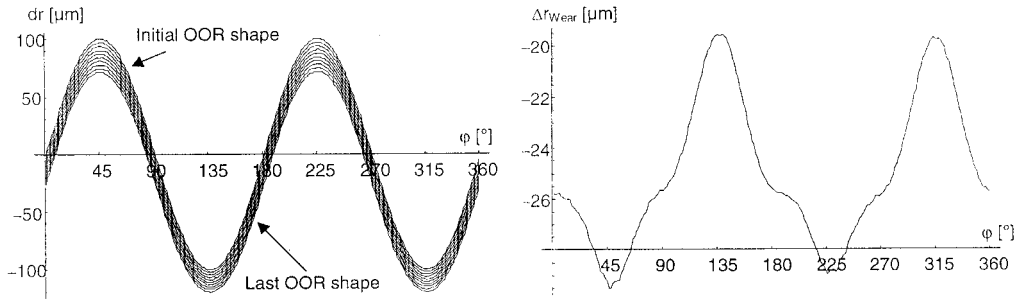

Figure 12. Long term wear development shown by the wheel shape changes dr (left graph) and the radius reduction Δr_{Wear} (right graph) as a function of the angle of wheel rotation φ as a consequence of an initial OOR wheel shape of the second order and a peak-to-peak radius deviation $r_{OOR} = 0{\cdot}2$ mm.

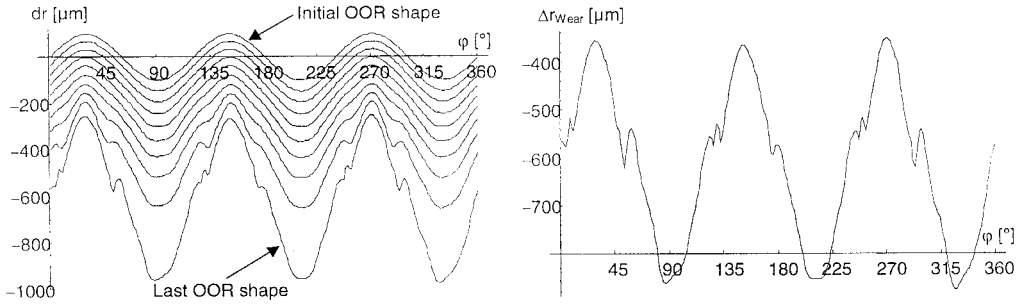

Figure 13. Long term wear development shown by the wheel shape changes *dr* (left graph) and the radius reduction Δr (right graph) as a function of the angle of wheel rotation φ as a consequence of an initial OOR wheel shape of the third order and a peak-to-peak radius deviation $r_{OOR} = 0{\cdot}2$ mm

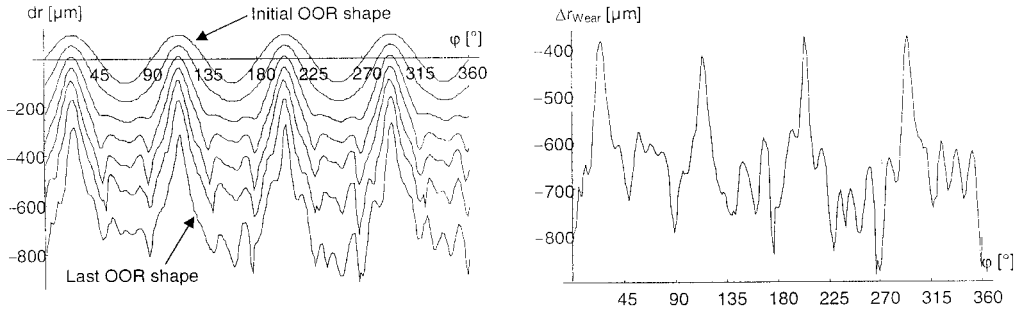

Figure 14. Long term wear development shown by the wheel shape changes *dr* (left graph) and the radius reduction Δr_{Wear} (right graph) as a function of the angle of wheel rotation φ as a consequence of an initial OOR wheel shape of the fourth order and a peak-to-peak radius deviation $r_{OOR} = 0{\cdot}2$ mm.

rotation φ. The right graph shows the radius reduction Δr_{Wear} during the long term wear simulation as the difference of the initial and the last profile. For all analyses the schedule of operating conditions in Table 2, the same roll-over factor c and 54 iterations (simulation of the fourth order OOR shape only 36 iterations) were used.

The lower graph in Figure 11 shows two excavation maxima at the falling and rising slope of the first OOR order radius curve while the excavation minimum coincides with the radius minimum. Because of the very small amount of material excavation a *very slow* change from an eccentricity (first OOR order) to a radius shape of the third OOR order can be noticed.

The material excavation curve as consequence of the second order OOR shape in Figure 12 shows also a coincidence of the excavation minima with the radius minima so that no enlargement of this OOR order can be expected. In the long run the radius maxima will be decreased *very slowly* and the second order shape will change *gradually* to the forth order radius deviation.

In Figure 13 the *rapid* enlargement of OOR shapes of the third order without changes in shape and phase can be seen. The excavation maxima coincide with the radius minima and *vice versa* so that the enlargement process will continue. The higher harmonics at the falling and rising slopes are caused by the wheel–rail lift–off at these locations where the wheel hits the rail again. They can be observed on both slopes caused by the different vehicle directions and start growing within the simulation when the system becomes strongly non-linear by normal force variations of a similar size to the static load.

OOR shapes of the fourth order shown in Figure 14 lead to higher harmonic OOR orders with a certain enlargement of the initial OOR amplitude. Similar results can be observed by the fifth order OOR shape which is not shown.

The comparisons of the wear progress as a consequence of four different initial radius deviations show that during the same period of time under the same operating conditions the third order OOR shape with an peak-to-peak OOR amplitude of the manufacturing/maintenance tolerance $r_{\mathrm{OOR}} = 0{\cdot}2$ mm exceeds the operating tolerance while the first and second order OOR shapes do not change significantly. The fourth order OOR shape changes significantly to higher orders.

All the described phenomena depend on the track properties as well as on the excitation frequency f_{OOR} which is the product of the frequency of wheel rotation and the OOR order. For this reason, other typical OOR orders can be expected in different typical speed ranges of a vehicle and/or on different substructure.

3.4. CLASSIFICATION OF OOR ORDERS

Because of the described phase shift of the lateral wear energy three significant frequency ranges can be classified: for low frequencies (range 1), medium ones (range 2) and high ones (range 3). Within range 1 and 3 both excavation maxima are located at the falling and rising slopes of the radius curve aside of the minimum of the OOR shape. An enlargement of the existing OOR order will not occur in these two ranges. The shape will change to higher harmonic orders. The

speed of these changes depends strongly on the normal force variations between wheel and rail at the specific excitation frequency. For medium frequencies (range 2) the two excavation maxima occur approximately at the maximum and at the minimum of the OOR shape. Because of the higher excavation at the radius minimum the OOR shape enlarges rapidly without changing its OOR order or phase.

No precise limits for the frequency ranges can be given because they strongly depend on the track properties. In the case of an ICE-1 which is running on a "stiff" track the medium range 2 is approximately limited by 50 and 80 Hz.

4. CONCLUSIONS

Even small wheel radius deviations within the manufacturing/maintenance tolerance cause considerable variations of the normal forces between wheel and rail on "stiff" substructures and modern high speed tracks of the Deutsche Bahn AG, respectively. These normal force variations depend mainly on the excitation frequency which is defined as the product of the rotational frequency of the wheel and the number of out-of-round periods over the wheel circumference (OOR order). At high speeds the normal force variations at wheels with the third or the fourth order radius deviation reach very large amplitudes. For these operating conditions even radius deviations within the operating tolerance cause a periodical wheel–rail lift-off. For "softer" substructures the normal force variations are significantly smaller and no periodical wheel–rail lift-off can be observed within the operating conditions.

These large normal force variations accelerate the wheel vertically and excite a bending oscillation of the wheelset axle. Within the frequency range considered the wheel disk can be assumed to be stiff and rigidly coupled to the axle. Consequently, the bending motion of the axle causes lateral slip and lateral material excavation between wheel and rail. Longitudinal material excavation due to longitudinal slip and spin plays a minor role.

Within the high speed range and based on the assumed track properties the long term wear progress of different sinusoidal radius deviations with one to five OOR periods over the wheel circumference has been investigated. Among them only OOR shapes of the third order enlarge rapidly without changing their shape or location on the wheel. Radius deviations of the first and the second order cause only small normal force variations and consequently only slight material excavation. The first order OOR shape changes very slowly to the third order while the second order shape changes very gradually to the fourth order OOR shape. The fourth and the fifth order OOR shapes cause very large normal force variations and change with a considerable speed to higher harmonics.

The results described depend strongly on the track properties and the excitation frequency so that within a different typical speed range and/or on different substructure characteristic other typical OOR orders can be expected.

REFERENCES

1. P. MEINKE and S. MEINKE 1997 *(TAT-Anteil) Schlußbericht, IAT*-019, *Starnberg*. Forschungsvorhaben Unrundheiten an Eisenbahnrädern.
2. *ADAMS/Solver Reference Manual* 8.0 1994 Ann Arbor; Mechanical Dynamics Inc.
3. DÖLL GELLES AHNERT 1996 *Bericht MSM*/0836/08/96 *der Thyssen Henschel Magnetfahrtechnik, Kassel*. Prüfprotokoll, Ermittlung von Biege- und Torsionseigen-frequenzen einer Radsatzwelle mit Scheibenrädern der Bauart 14.
4. W. KIK and H. STEINBORN 1987 *ILR Mitt*. 112, *Institut für Luft- und Raumfahrt der technischen Universität Berlin, Berlin*. Quasistationärer Bogenlauf-Mathematisches Rad/Schiene Modell.
5. J. J. KALKER 1982 *Vehicle System Dynamics* **11** A farst algorithm for the simplified theory of rolling contact.
6. J. J. KALKER 1990 *Three-Dimensional Elastic Bodies in Rolling Contact*. Dordrecht: Kluwer Academic Publishers.
7. M. ZACHER 1996 *ETR Heft* **10**, 605–610, Unrunde Räder und Oberbausteifigkeit.
8. M. EIPERT 1992 *Bericht Aktenzeichen* 108*a*. 10809 *lo der Deutschen Bundesbahan, München*. Rechnerische Bestimmung der Gleissteifigkeit in horizontaler Richtung.
9. U. PAHNKE 1994 *Erster Zwischenbericht zum Forschungs-vorhaben Unrundheiten an Eisenbahnrädern, Starnberg*. Eingrenzung vertikaler Oberbauparameter und Abschätzungen zur Radsatzschwingung auf dem Oberbau.
10. T. M. BEAGLEY 1975 *Wear* **36**, 317–335. Severe wear of rolling-sliding contacts